International Journal of Progressive Research in Science and Engineering
Volume-1, Issue-4, July-2020
www.ijprse.com

New proportional resonant control scheme for Grid connected Inverters under Unbalanced and Distorted Grid Conditions

Devi N[1], KNSK Santhosh [2]

[1]PG Student, Department of EEE, Kakinada Institute of Science and Technology, Kakinada, Andhra Pradesh India.

[2]Asst. Professor, Department of EEE, Kakinada Institute of Science and Technology, Kakinada, Andhra Pradesh India.

Corresponding Author: devinaralasetti20@gmail.com

Abstract: - This paper deals the grid voltage, especially grid voltage under balanced, unbalanced and harmonically distorted grid conditions, often distorts the injected currents of grid-connected inverters. To address this problem, a robust control scheme of grid-connected inverters is presented in this project. The proposed control scheme employs open-loop filtering technique to offer exact steady-state performance as well as fast transient response. The proposed resonant controller is developed for the inner current control loop of the system. The proposed controller has the ability to track ac current with zero steady-state error. The outer dc-link voltage control loop is developed through the indirect vector control method at synchronously rotating reference frame. The control scheme ensures improved performance of the system at variable load disturbances. The control scheme is implemented in MATLAB–SIMULINK environment.

Key Words—***Resonant controller,***

I. INTRODUCTION

GRIDs connected converters are important in renewable energy systems. In this context, the control of the grid injected current is a relevant problem, which becomes challenging due to the uncertainty of the grid impedance at the point of common coupling. In grid-connected converters, *LCL* filters are frequently used to interface PWM inverters and the grid, in order to attenuate the harmonics from the PWM signal. One problem that arises then is the need of attenuation of the high resonance peak from *LCL* filters.

One solution is given by passive damping strategies [61] and another is given by active damping, which is based on the design of a suitable controller able to damp the resonance without inserting elements in the filter. Among the active damping strategies in current control, it is worth to mention the proportional–integral controllers in synchronous reference frame (SRFPI) and the proportional resonant (PR) controllers in a stationary reference frame. SRFPI controllers are based on the design of PI controllers in a synchronous reference frame for three-phase systems [62], using filter-based strategies [14], [15] or multiloop strategies [63]–[64]. For PR controllers, the design in a stationary frame is commonly used to provide an infinite gain at chosen frequencies in order to ensure tracking for sinusoidal references and to reject specific harmonic disturbances [65]–[67]. SRFPI controllers are known to have an easy design, but present a poor harmonic rejection capability, especially for high-frequency harmonics.

On the other hand, PR controllers can lead to a good harmonic rejection with the inclusion of more resonant in the controller, with the cost of computing more control gains. Alternatives are given, by proportional complex integral control in [68] and also by feedforward strategies, capable to suppress the effect of grid-voltage harmonics, but without reducing the phase margin. Other alternatives for the control of PWM grid-connected converters are given in the state space, based on linear quadratic controllers, as in [69] and [70], which may suffer from the difficulties of choice for the cost function weighting matrices, and also based on pole location techniques, as in. All strategies previously mentioned do not take into account a priori robustness in the design of the control gains. This issue is taken into account in. Robust multi objective control schemes using adaptive and deadbeat structures can be found in [70] and [71]. Robust predictive control can be seen in [74] and [76], where the robust predictive controller works in parallel with an adaptive strategy to improve the stability of the predictive controller.

The other application of adaptive controllers for grid-connected converters with LCL filters is shown in [73], where a model robust adaptive controller ensures tracking and robust performance for the grid with parameter uncertainties. In [34], $H\infty$ repetitive controllers are used for voltage control to cope with grid frequency variations. Other works have dealt with robust control design for grid-connected converters with *LCL* filters by means of linear matrix inequalities (LMIs). In, partial state feedback is used to provide robustness to grid parametric uncertainty. The controller is associated with resonant controllers to ensure the tracking of sinusoidal reference and reject specific harmonics disturbances. This study shows the viability of using LMIs to get robustness for this application, being the resonant control design dependent on a procedure in the frequency domain.

International Journal of Progressive Research in Science and Engineering
Volume-1, Issue-4, July-2020
www.ijprse.com

II. CONTROL TECHNIQUE

The proposed resonant control strategy is divided into two cascaded control loops: (A) dc-link voltage control loop, and (B) inner M-PR current control loop.

A. DC-link Voltage controller

Fig. 1 explains that the d-axis current reference, i_d^* ,is generated by the voltage controller through processing of the error between the present dc-link voltage and its corresponding provided reference value.

$$i_d^* = [V_{dc}^* - V_{dc}](K_{pdc} + K_{rdc}/s) \quad (1)$$

Where DC-link voltages V_{dc} represent the present dc-link capacitor voltage of the inverter. With the controller PI, the dc-link voltage loop has the transfer function as:

$$C_{PI}(s) = \left(\frac{R_1}{R_1Cs+1}\right)\left(\frac{K_{pdc}s + K_{rdc}}{s}\right) = \frac{R_1K_{pdc}s + R_1K_{rdc}}{s(R_1Cs+1)} \quad (2)$$

where R is the leakage resistances of dc-link capacitors of the PV system. The controller gains are designed to be of K_{pdc} = 0.622 and K_{rdc} = 0.0014. Equation (2) is found out to be same for both of the inverters, and the numeric values are used to produce

$$C_{PI}(s) = \frac{16790s + 37.7}{44.55s^2 + s} \quad (3)$$

B. Current controller:

The current control is implemented through M-PR current controller. The M-PR current controller is adopted due to its robust and fast dynamic response to perturbations. The gate signals for inverter are generated by sinusoidal pulse width modulation topology, where the switching frequency is c as f_s = 150 Hz. The inverter modulating signals are phase shifted by 180∘. The proposed M-PR controller for the transformer output currents are developed in stationary reference frame using the $abc \rightarrow \alpha\beta$ conversion. The ideal-PR controller is represented by

$$C_{ideal-PR}(s) = \frac{Y(s)}{E(s)} = K_P + \frac{2K_r s}{s^2 + \omega_0^2} \quad (4)$$

Where K_p, ω_0, and K_r are the proportional gain, the resonant frequency, and resonant gain, respectively. The design of PR controller includes the tuning of four parameters, namely K_p, K_r, ω_c, and ω_0 $\omega_0 = 2\pi f_0$. The ideal-PR controller is challenged for implementation in reality since it operates as a network with infinite quality factor, which cannot be achieved in either analogue or digital system. Accordingly, for the realisation of PR controller, the transfer function of the M-PR controller, used in general by the authors in [12, 14] and [13, 33] is

$$C_{ideal-PR}(s) = \frac{Y(s)}{E(s)} = K_P + \frac{2K_r s}{s^2 + \omega_0^2} \quad (5.6)$$

In the design procedure of the M-PR controller, there are four main parameters to be considered; K_r, K_p, ω_c, and ω_0. Since ω_0 is the fundamental frequency of the system, it can be selected as $\omega 0 = 2\pi f 0 = 314.16$ *rad/s*. The control model of the inner current loop can be shown in Fig. 2, where $1/(0.5T_s + 1)$ is the first-order inertia link that represents the delay caused by the sampling; programme calculation and PWM control links, and T_s is the sampling time. When the feedforward compensation term of grid voltages is not considered, the open-loop transfer function of the inner loop can be obtained as

$$G_{oc}(s) = \left(K_p + \frac{2K_r\omega_c s}{s^2 + 2\omega_c s + \omega_0^2}\right)\left(\frac{1}{(0.5T_s s + 1)(Ls + R)}\right) \quad (5.7)$$

Then, the closed-loop transfer function is

$$G_{cc}(s) = \frac{i_\alpha,(\beta)}{i_\alpha,(\beta)ref} = \left(\frac{C_{M-PR}(s)}{C_{M-PR}(s) + (0.5T_s s + 1)(Ls + R)}\right) \quad (5.8)$$

For $s = j\omega_0$, the following relationship can be obtained

$$G_{cc}(s) = \frac{i_\alpha,(\beta)(j\omega_o)}{i_\alpha,(\beta)ref\,(j\omega_o)} = 1 \quad (5.9)$$

Thus, it is known that, when the resonant frequency ω_0 of M-PR controller is equal to the angular frequency of controlled object, the input currents can track reference values without steady-state errors.

C. Implementation of resonant controller:

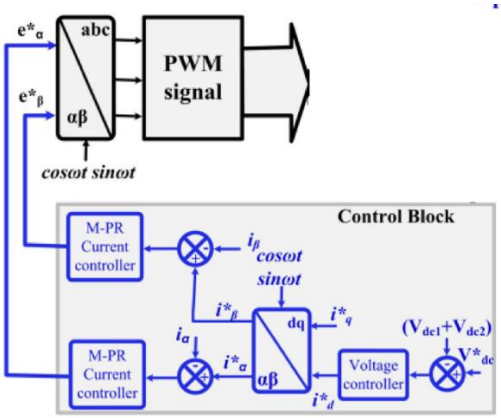

Fig. 5.1: Proposed resonant controller

The K_r is chosen to eliminate the phase and magnitude steady-state errors at low and high frequencies. The cut-off frequency ω_c is chosen to provide a permitted bandwidth around the resonant frequency. The PQ

International Journal of Progressive Research in Science and Engineering
Volume-1, Issue-4, July-2020
www.ijprse.com

standard of Macau and Hong Kong states that, the limit of frequency deviation Δf is ±2%, where ω_c can be calculated from the expression $\omega_c = 2\pi f_0 \Delta f$ [12]. Accordingly, ω_c can be found as 6.28 rad/s for $f_0 = 50$ Hz. However, the stability margin will be reduced with the increment in K_p. The main objective of employing the M-PR controller is to generate $e\alpha*$ and $e\beta*$by processing the load current error $i*\alpha - i\alpha$ and $i\beta* - i\beta$ at its input. It is well known that, while Kp affects the dynamics of this process, the Kr significantly reduces the steady-state error in $i\alpha$ and $i\beta$, and determines the bandwidth centred at the fundamental frequency (50 Hz) [13]

III. Proposed System

To suppress the grid voltage disturbances due to imbalance and harmonic distortion, it is more effective to use the SRF rather than the stationary reference frame [17]. The transformation between abc- and qd-frame is done by means of Park's transformation [25]. Fig. 5.1 shows the proposed control scheme for a three-phase grid-connected inverter interfaced with the utility grid through an LCL filter. R_1, R_2, L_1, and L_2 represent the resistances and inductances of the filters, respectively, C_f represents the filter capacity, and Lg represents the grid inductance. The inverter is controlled by the proposed current controller through the space vector pulse width modulator (PWM) [26]. Also, the proposed PLL scheme is used to facilitate the grid synchronization. The proposed current controller and PLL scheme will be presented in detail in section III. The continuous-time representation of the inverter can be expressed in the SRF which rotates synchronously with the angular speed of grid voltage ω_g as

$$x_c(t) = A_c x_c(t) + B_c u_c(t) + B_{cd} w_c(t) \quad (5.1)$$

$$y(t) = C_c x_c(t) \quad (5.2)$$

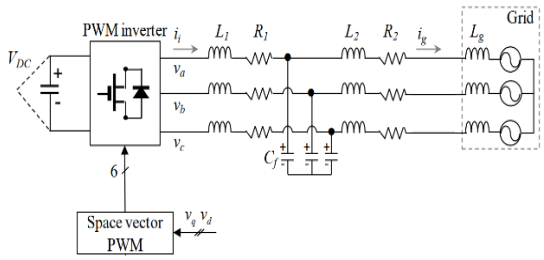

Fig. 2. Configuration of an LCL-filtered three-phase grid-connected inverter: power circuit and proposed control scheme.

IV. Results And Discussion

Also, both the PI-RES controller and the extended controller of [24] are synchronized with the grid using the SRF-PLL. Fig. 3 and Fig. 4 show the simulation results under unbalanced and distorted grid voltages using three control schemes. As can be observed, under a step change of q-axis reference current of 3 A, the settling time for three control schemes is more or less the same with 10 msec. Nevertheless, the PI-RES controller with the SRF-PLL, and the extended controller of [14] with the SRF-PLL suffer severe oscillation during transient periods, which may lead to the degradation of grid power quality as well as ineffective use of primary power sources. Also, as is clearly shown in Fig.4, the proposed control scheme offers the highest quality of injected currents. To investigate the influence of the proposed PLL scheme on the current control, Fig. 4 shows the simulation results for current responses when three PLL schemes are applied to the proposed current controller under +10° phase angle transition of unbalanced and distorted grid voltage.

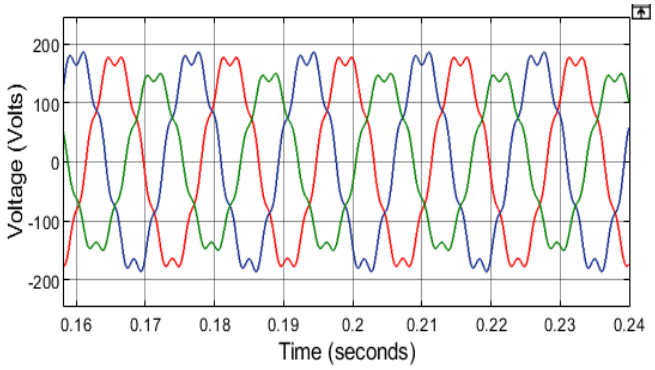

Fig. 5.3(a)

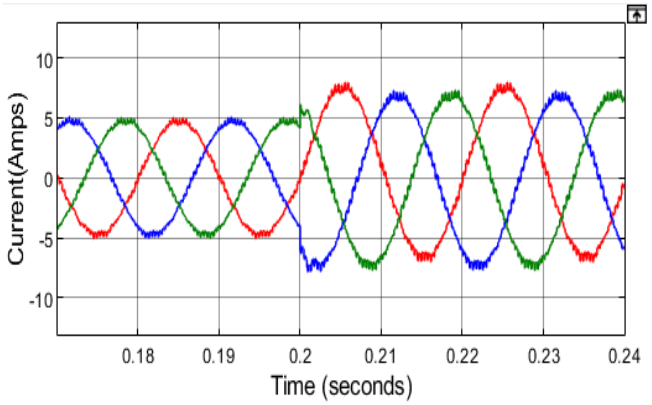

Fig. 5.3(b)

International Journal of Progressive Research in Science and Engineering
Volume-1, Issue-4, July-2020
www.ijprse.com

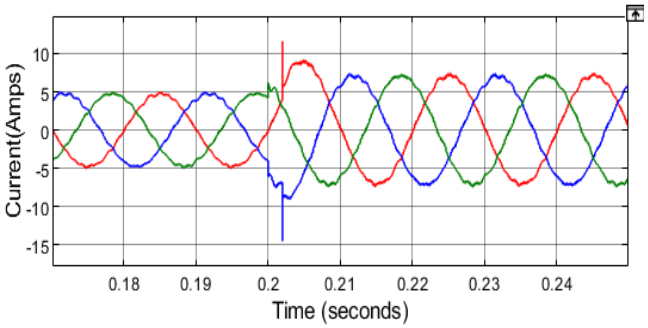

Fig. 5.3(C)

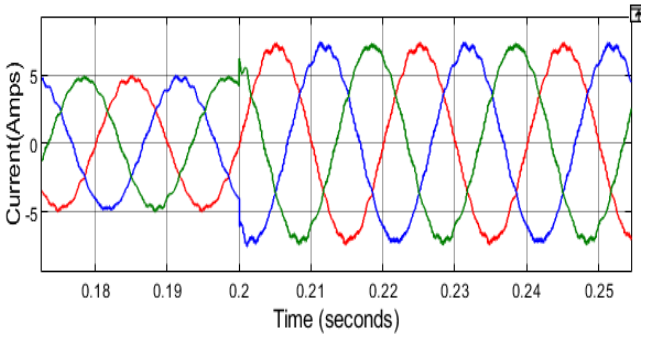

Fig. 5.3(d)

Fig.3. Simulation results of transient response under unbalanced and distorted grid voltages: (a) three-phase unbalanced and distorted grid voltages; (b) PI-RES controller with the SRF-PLL; (c) extended controller of [24] with the SRF-PLL; (d) proposed control scheme.

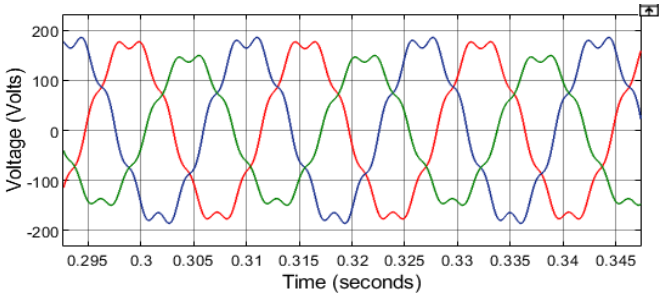

Fig. 5.4(a)

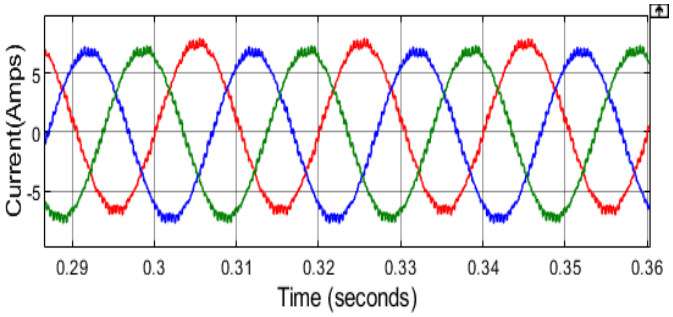

Fig. 5.4(b)

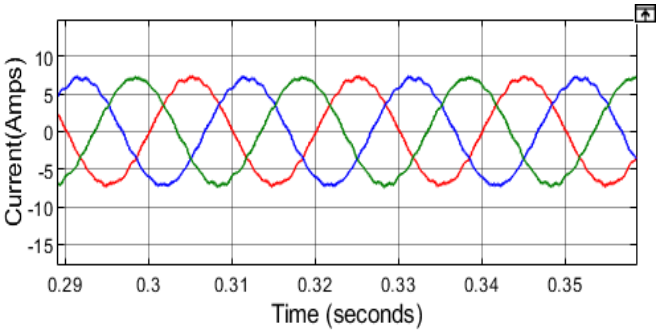

Fig. 5.4(c)

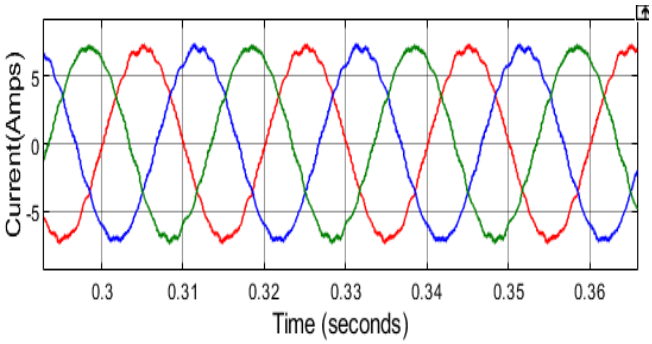

Fig. 5.4(d)

Fig. 4: Simulation results under unbalanced and distorted grid voltages: (a) three-phase unbalanced and distorted grid voltages; (b) PI-RES controller with the SRF-PLL; (c) extended controller of [24] with the SRF-PLL; (d) proposed control scheme.

V. CONCLUSION

In this project, a robust control scheme for grid-connected inverters with LCL filter under unbalanced and distorted grid conditions has been presented. The proposed scheme ensures harmonic-free injected currents and smooth transient response even under severely abnormal grid voltages. Here, the performance of the control is found to be satisfactory in all the considered operating conditions. The salient features of the proposed scheme include the following: (i) maintains the dc-link voltage at the desired level to extract power from the solar PV modules, (ii) isolated dual-inverter dc-link connected PV source is used to produce multilevel output voltages

The effectiveness and feasibility of the proposed control scheme are verified with a MATLAB Simulink. It is found that all of the simulation results in both transient and steady-state closely match with the existing system results throughout the operation in stand-alone mode. The grid-connected mode of operation is also tested in simulation environment and is found to be capable of delivering power

according to the availability in input. The THD has been kept within the limit of grid connection standard.

REFERENCES

[1] A. M. Bouzid, J. M. Guerrero, A. Cheriti, M. Bouhamida, P. Sicard, and M. Benghanem, "A survey on control of electric power distributed Generation systems for microgrid applications applications" *Renewable and Sustainable Energy Reviews*, vol. 44, pp. 751-766, Apr. 2015.

[2] I. Patrao, E. Figueres, G. Garcera, and R. Gonzalez-Medina, "Microgrid architectures for low voltage distributed generation," *Renewable and Sustainable Energy Reviews*, vol. 43, pp. 415-422, Mar. 2015.

[3] IEEE Std. 1547-2003, "*Standard for interconnecting distributed resources with electric power systems*," IEEE, ISBN 0-7381-3720-0SH95144, Jun. 2003.

[4] S. Chung, "A phase tracking system for three phase utility interface inverters," *IEEE Trans. Power Electr.*, vol. 15, no. 3, pp. 431 – 438, May. 2000.

[5] F. Blaabjerg, R. Teodorescu, M. Liserre, and A. V. Timbus, "Overview of control and grid synchronization for distributed power generation systems," *IEEE Trans. Indus. Electron.*, vol. 53, no. 5, pp. 1398-1409, Oct. 2006.

[6] S. Golestan, M. Ramezani, J. M. Guerrero, F. D. Freijedo, and M. Monfared, "Moving average filter-based phase-locked loops: performance analysis and design guidelines," *IEEE Trans. Power Electr.*, vol. 29, no. 6, pp. 2750-2763, Jun. 2014.

[7] E. Robles, S. Ceballos, J. Pou, J. L. Martin, J. Zaragoza, and P. Ibanez, "Variable-frequency grid-sequence detector based on a quasi-ideal lowpass filter stage and a phase-locked loop," *IEEE Trans. Power Electr.*, vol. 25, no. 10, pp. 2552 – 2563, Oct. 2010.

[8] F. Freijedo, J. Doval-Gandoy, O. Lopez, and E. Acha, "A generic open loop algorithm for three-phase grid voltage/current synchronization with particular reference to phase, frequency, and amplitude estimation," *IEEE Trans. Power Electr.*, vol. 24, no. 1, pp. 94-107, Jan. 2009.

[9] S. Golestan, J. M. Guerrero, and A. M. Abusorrah, "MAF-PLL with phase-lead compensator," *IEEE Trans. Indus. Electron.*, vol. 62, no. 6, pp. 3691-3695, Jun. 2015.

[10] Z. Yao, L. Xiao, and J. M. Guerrero, "Improved control strategy for the three-phase grid-connected inverter," *IET Renewable Power Generation*, vol. 9, no. 6, pp. 587 – 592, Jan. 2015.

[11] D. N. Zmood, and D. G. Holmes, "Stationary frame current regulation of PWM inverters with zero steady-state error," *IEEE Trans. Power Electr.*, vol. 18, no. 3, pp. 814 – 822, May. 2003.

[12] J. C. Vasquez, J. M. Guerrero, M. Savaghebi, J. Eloy-Garcia, and R.Teodorescu, "Modelling, analysis, and design of stationary-reference frame droop-controlled parallel three-phase voltage source inverters," *IEEE Trans. Indus. Electron.*, vol. 60, no. 4, pp. 1271 – 1280, Apr. 2013.

[13] R. Teodorescu, F. Blaabjerg, M. Liserre, and P. C. Loh, "Proportional resonant controllers and filters for grid-connected voltage-source converters," *IEE Proceedings - Electric Power Applications*, vol. 153, no. 5, pp. 750 – 762, Sep. 2006.

[14] M. Castilla, J. Miret, A. Camacho, J. Matas, and L. G. de Vicuña, "Reduction of current harmonic distortion in three-phase grid-connected photovoltaic inverters via resonant current control," *IEEE Trans. Indus. Electron.*, vol. 60, no. 4, pp. 1464 – 1472, Apr. 2013.

[15] X. Yuan, W. Merk, H. Stemmler, and J. Allmeling, "Stationary-frame generalized integrators for current control of active power filters with zero steady-state error for current harmonics of concern under unbalanced and distorted operating conditions," *IEEE Trans. Indus. Appl.*, vol. 38, no. 2, pp. 523 – 532, Mar. 2002.

[16] M. Liserre, R. Teodorescu, and F. Blaabjerg, "Multiple harmonics control for three-phase grid converters systems with the use of PI-RES current controller in a rotating frame," *IEEE Trans. Power Electr.*, vol. 21, no. 3, pp. 836 – 841, May 2006.

[17] R. I. Bojoi, G. Griva, V. Bostan, M. Guerriero, F. Farina, and F. Profumo, "Current control strategy for power conditioners using sinusoidal signal integrators in synchronous reference frame," *IEEE Trans. Power Electr.*, vol. 20, no. 6, pp. 1402 – 1412, Nov. 2005.

[18] S. W. Kang and K. H. Kim, "Sliding mode harmonic compensation strategy for power quality improvement of a grid-connected inverter under distorted grid condition," *IET Power Electr.*, vol. 8, no. 8, pp. 1461 – 1472, Feb. 2015.

[19] Q. C. Zhong and T. Hornik, "Cascaded current-voltage control to improve the power quality for a grid-connected inverter with a local load," *IEEE Trans. Indus. Electron.*, vol. 60, no. 4, pp. 1344 – 1355, Apr. 2013.

[20] Y. Jia, J. Zhao, and X. Fu, "Direct grid current control of *LCL*-filtered grid-connected inverter mitigating grid voltage disturbance," *IEEE Trans. Power Electr.*, vol. 29, no. 3, pp. 1532 – 1541, Mar. 2014.

[21] Y. A. I. Mohamed, "Mitigating of dynamic, unbalanced, and harmonic voltage disturbance using grid-connected inverters with *LCL* filter," *IEEE Trans. Indus. Electron.*, vol. 58, no. 9, pp. 3914 – 3924, Sep. 2011.

[22] J. R. Fischer, S. A. Gonzalez, I. Carugati, M. A. Herran, M. G. Judewicz, and D. O. Carrica, "Robust predictive control of grid-tied converters based on direct power control," *IEEE Trans. Power Electr.*, vol. 29, no. 10, pp. 5634 – 5643, Oct. 2014.